PCCP

Accepted Manuscript

ROYAL SOCIETY OF CHEMISTRY

www.rsc.org/pccp

Physical Chemistry Chemical Physics

RSCPublishing

PAPER

Towards Comprehensive Insight into Efficient Hydrogen Production by Self-Assembled $Ru(bpy)_3^{2+}$-Polymer-Pt Artificial Photosystems

Cite this: DOI: 10.1039/x0xx00000x

Received 00th January 2015,
Accepted 00th January 2015

DOI: 10.1039/x0xx00000x

www.rsc.org/

Huan Lin, Dan Liu, Jinlin Long*, Zizhong Zhang, Huaqiang Zhuang, Yi Zheng, Xuxu Wang*

This work studied in detail the role of polymers in the artificial photosystems composed of tris (2, 2'-bipyridyl) ruthenium (II) chloride ($Ru(bpy)_3Cl_2$) as a photosensitizer (PS), colloidal platinum stabilized by polyanions (polyanion-Pt) as hydrogen-evolving catalysts, and sodium ascorbate (NaHA) as an electron donor without adding a traditional molecular type of electron mediator, and achieved some comprehensive insights into the visible-light-induced hydrogen production. Several polymers, including neutral polyvinylpyrrolidone (PVP), anionic poly (sodium 4-styrenesulfonate) (PSS) and poly (acrylicacid) (PAA), were well-established to not only work for the stabilization of Pt NPs, but also be effective for the hydrogen production. Under the optimal conditions, an outstanding apparent quantum efficiency of 12.8 % for hydrogen evolution was achieved. The formation of a self-assembled and spatially-separated donor-acceptor complex by the non-covalent intermolecular interaction between PS and polymer-Pt was pivotal for the solar-to-hydrogen conversion at high efficiency. The important details of photo-induced electron- and energy-transfer processes in the self-assembled artificial photosystem were uncovered by nanosecond transient absorption and time-resolved fluorescence spectroscopies. The initial step of the photocatalytic H_2 production is a reductively-quenching of the triplet excited state PS by NaHA, leading to the reduced form of PS, which can be quenched quickly by polymer. The determining-rate step is the electron transfer from PS to catalyst via the polymer bridge.

1. Introduction

Since Lehn[1] reported the first artificial photosynthesis system based on $Ru(bpy)_3^{2+}$ as a photosensitizer (PS) and Pt nanoparticles (NPs) as a hydrogen-evolving catalysts in early 1970s, followed closely by the similar scheme shown independently by Grätzel[2] and Okura[3], artificial photosynthesis for hydrogen evolution, which offers a facile way of solar-to hydrogen fuel (SHF) conversion, is widely considered as a particularly attractive route to the realm of hydrogen economy in the near future.[4-10] The molecular artificial hydrogen-producing systems usually consist of a photosensitizer, an electron mediator and a donor, and a hydrogen-evolving catalyst.[11-15] Its working mechanism is illustrated in Scheme 1, where PS such as $Ru(bpy)_3^{2+}$ absorbs light to generate a long-lived excited state. And then one electron is transferred *via* a mediator such as methyl viologen or $Rh(bpy)_2Cl_3$ to a hydrogen-evolving catalyst, where H^+ can obtain the electron to form molecular hydrogen. The oxidized $Ru(bpy)_3^{3+}$ is reduced by the sacrificial electron donor to regenerate $Ru(bpy)_3^{2+}$. The most important steps in the system are the photoinduced electron transfer from a photoexcited photosensitizer to a hydrogen-evolution catalyst. The direct

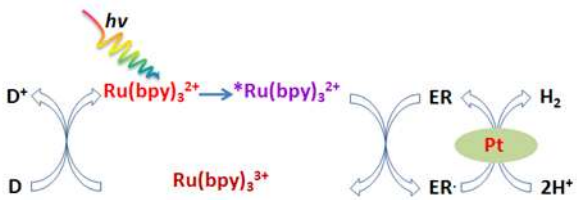

Scheme 1 Hydrogen evolution mechanism of early four-component artificial photosynthetic system based on $Ru(bpy)_3^{2+}$ as photosensitizer, colloidal platinum as catalyst, methyl viologen or $Rh(bpy)_2Cl_3$ as electron relays (ER), EDTA or TEA as electron donor (D).

electron injection from a photosensitizer to a catalyst generally led to a very low efficiency of hydrogen-production. The addition of an electron relay is an often-used strategy to accelerate the election transfer, and yet easily deactivates the multi-step electron-transfer system due to the significant energy loss and the dimerization or irreversible hydrogenation of the reduced electron relay.[16] This greatly limited the practical application of the hydrogen-production system with an electron mediator. Development of robust artificial photosynthetic systems that can work in the absence of electron mediators for

efficient SHF conversion has been a focus of research in the artificial photosynthesis community.

To improve efficiency of hydrogen production in homogeneous aqueous solutions of photocatalytic assemblies, tremendous efforts have been made to the search for photosensitizers with high quantum efficiency and molecular hydrogen-evolution catalysts over the past decades.[6, 8, 9, 17] Hitherto, a number of cobalt,[18-22] nickel,[23-26] and iron-based[27] molecular catalysts have been developed. The reduced species of molecular catalysts have a strong reducing capacity to reduce H_2O to H_2, but they commonly suffered from the poor photo-stability. Noble metals, especially Pt, still are widely applied as the hydrogen-producing catalysts to construct the three-component systems without the electron relay.[28-30] Owing to the heterogeneous environment, the electron transfer is severely blocked between PS molecules and bare Pt NPs. One solution is that PS is covalently or coordinatively attached to the catalyst.[31-33] Yang and coworkers suggested multibranched-porphyrin-functionalized Pt nanocomposites self-assembled by hydrogen-bonded interaction for photocatalytic hydrogen production.[34-36] But the quantum yield of hydrogen was achieved as low as 3.0% under visible light irradiation. Fukuzumi and coworkers[29, 30, 37] showed another solution of protecting metal NPs (M = Pt, Ru, Fe) with poly(*N*-vinyl-2-pyrrolidone) (PVP-M), and pioneered an enzymatic system for photocatalytic H_2 production using PVP-M as hydrogen-evolving catalysts and Acr^+-Mes or $QuPh^+$-NA as PS. In the micro-heterogeneous photosystem, the photocatalyst undergoes photo-induced electron transfer from the Mes or NA moieties to the singlet excited states of the corresponding $Acr^{+\cdot}$ and $QuPh^{+\cdot}$ moieties to produce an extremely long-lived electron transfer state, which is capable of oxidizing NADH and reducing Pt-PVP, leading to the efficient hydrogen evolution. A fast electron injection mechanism was generally proposed for the artificial photosystems composed of PS, polymer-functionalized Pt catalysts, and sacrificial electron donor. Such an explanation seems to be expedient. Several important scientific issues for the three-component photosystems need to be further clarified: What is responsible for the smooth electron transfer between PS and the hydrogen-evolving catalyst? What is the real role of the polymer? The objective of the work is to complement these missing details.

Herein, we constructed an artificial photosystem based on $Ru(bpy)_3^{2+}$ as a photosensitizer (PS), polyanion-capped Pt NPs as catalysts, and NaHA as a sacrificial electron donor for photocatalytic efficient hydrogen evolution, without adding a traditional molecular type of electron relay species. In this photosystem, $Ru(bpy)_3^{2+}$, polymer-Pt, and NaHA can be simply self-assembled to *in situ* form a spatially-separated donor-acceptor complex, achieving the higher efficiency of electron transfer from PS to catalyst. A high quantum efficiency of hydrogen can be achieved up to 12.8% under visible-light. Various experimental parameters affecting the hydrogen production are investigated, including the type of polymers, the size of the Pt NPs, pH and the concentration of components. Such a system avoids a traditional molecular electron mediator, and inherently eliminates energy losses and back reactions associated with the electron transfer to the relay. The function of polymers as molecular wires was highlighted in this work. A comprehensive insight into the efficient hydrogen evolution was achieved, and this in turn has led us to develop more robust artificial photosystems for future application.

2. Experimental

2.1 Materials

Tris (2, 2'-bipyridyl) ruthenium (II) chloride hexahydrate ($Ru(bpy)_3Cl_2\cdot 6H_2O$) and L-ascorbic acid sodium salt (NaHA) were obtained from Alfa Aesar. Hexachloroplatinic (IV) acid hexahydrate ($H_2PtCl_6\cdot 6H_2O$), poly (acrylic acid) (PAA, MW: 450,000) and polyacrylamide (PAM, MW: 2×10^6-14×10^6) were purchased from Aladdin Industrial Corporation. Ethylene glycol, polythylene glycol (PEG, MW: 2000) and polyvinylpyrrolidone (PVP, K-30, MW: 40000) were purchased from Sinopharm Chemical Regent Co., Itd. Poly (ethylene glycol)-block-poly (propylene plycol)-block-poly (ethylene glycol) (PEG-PPG-PEG, P123, Mn ~ 5800) was purchased from Energy Chemical Co. Poly (sodium 4-styrenesulfonate) (PSS, MW: 70,000) and poly(ethyleneimine) solution (PEI, average M_n ~ 60,000 by GPC, average M_w ~ 750,000 by LS, 50 wt,% in water) were purchased from Sigma-Aldrich Corporation. All chemicals were of analytical grade.

2.2 Preparation of Polymer-Modified Pt Colloids

The platinum colloidal solutions were prepared according the to previous method with some improvements.[38] In a 100 ml Schlenk flask, 0.5 ml $H_2PtCl_6\cdot 6H_2O$ (2.56×10^{-5} mol) aqueous solution was added to 25 ml ethylene glycol solution containing 8 mM NaOH under magnetic stirring, where ethylene glycol acted as both a reduction reagent and a solvent without additional reductant.[39] The mixed solution was sealed and evacuated, followed by ultrasonic bath for 5 min at room temperature. After that, the sealed Schlenk flask was placed in the center of a microwave oven (Galanz WP 800SL23-3). After microwave irradiation at the maximum power output of 800 W for only 25 s, the solution changed from pale orange to dark brown. Then the ethylene glycol solution of Pt colloids was obtained. The fresh Pt colloids were added to 5-fold volume of water, PVP, PAM, PEG, P123, PSS, PAA and PEI aqueous solutions, respectively. The resultant catalysts are denoted as "Pt", "PVP-Pt", "PAM-Pt", "PEG-Pt", "P123-Pt", "PSS-Pt" "PAA-Pt" and "PEI-Pt" respectively.

The size-controlled PVP-Pt_n (n is the calculated average numbers of Pt atoms) nanoparticles (NPs) were prepared by a procedure similar to the Pt colloids synthesis above. Except that 0.139 g PVP (K-30) was added into the mixed solution prior to reaction, and the different NaOH concentrations are used to control the size of Pt NPs (12 mM for PVP-Pt_{60} with 1.2 nm, 10 mM for PVP-Pt_{75} with 1.3 nm, 8 mM for PVP-Pt_{95} with 1.4 nm,

7.2 mM for PVP-Pt_{115} with 1.5 nm and 4 mM for PVP-Pt_{276} with 2.0 nm).

2.3 Catalyst Characterizations

X-ray diffraction (XRD) pattern of the sample was collected on a Bruker D8 Advance X-ray diffractometer with Cu Kα radiation. The accelerating voltage and the applied current were 40 kV and 40 mA, respectively. Transmission electron microscopy (TEM) images and high-resolution TEM (HRTEM) images were obtained by a JEOL model JEM 2010 EX instrument at the accelerating voltage of 200 kV. The histograms of the particle size distribution were obtained on the basis of the statistic measurement in an arbitrary chosen area. The zeta potentials (ξ) of polymer-Pt colloids were determined by dynamic light scattering analysis (Zeta sizer 3000HSA) at 30 ˚C. The pH adjustment was achieved using HCl or NaOH aqueous solution when the zeta potential of the sample was measured as a function of pH.

2.4 Photophysical Measurement

UV-Vis diffuse reflectance spectra were measured with a Varian Cary 500. Photoluminescence emission spectra and photoluminescent lifetimes were measured at room temperature on a FL/FS920 spectrofluorimeter (Edinburgh Instruments) fluorescence spectrometer. The triplet transient difference absorption spectra and lifetimes were measured on an Edinburgh LP920 laser flash photolysis spectrometer. The excitation pump source was the Vibrant LD 355 II Nd: YAG/OPO system. The excitation wavelength was 450 nm for all of the samples unless otherwise noted. For each measurement, optically dilute (OD= 0.3-0.5) solutions were degassed by purging with a stream of N_2 gas for about 10 min and the head space of the solutions were maintained under positive N_2 pressure during data acquisition.

2.5 Photocatalytic Hydrogen Evolution

Photocatalytic reactions were conducted in a gas-closed circulation system with a side window Pyrex cell. 150 ml aqueous solution containing $Ru(bpy)_3Cl_2$ (66.7 μM), NaHA (50 mM), Pt colloids (167 μM) and polymer (667 μM as a monomeric unit) were added into the side-irradiation Pyrex reaction vessel, where the pH value of the solution was determined by a pH meter (Oakton Double Junction Waterproof pH Tester 30; resolution 0.1 pH, accuracy ± 0.01 pH; Eutech [Oakton] Instruments, Vernon Hills, IL, USA) and adjusted in a pH range of 2.0-10.0 by using NaOH (aq) or HCl (aq) without buffer. The reaction system was evacuated several times by a mechanical pump to remove air and nitrogen. The catalyst was dispersed uniformly in the aqueous solution under magnetic stirring and irradiated under a 300 W Xe lamp with a 420 nm cut-off filter at 283 K. The evolved hydrogen gas was circulated with a gas pump and quantified by an online gas chromatograph (Shimadzu, GC-8A, TCD, Ar carrier).

The apparent quantum yield for hydrogen production was measured under the same photocatalytic reaction. The amount of H_2 formed during 1 h of photocatalytic reaction under different wavelengths of 420, 450, 475, 500, 525, and 550 nm was used to calculate the quantum efficiency (QE) using the equation below:

$$\mathrm{QE}\,[\%] = \frac{2 \times \text{the number of evoleved hydrogen molecules}}{\text{the number of incident photons}} \times 100\%$$

3. Results and Discussion

3.1. Screening of Modifiers for Pt NPs

A series of water soluble nonionic polymers including PVP, PAM, PEG, and P123 and ionic polymers such as PSS, PAA, and PEI are used as modifiers for Pt NPs to examine their roles in photocatalytic hydrogen production. The chemical structures of all the polymers are displayed in Scheme 2. The PVP-Pt colloidal solution shows a pale yellow-brown color, while all of other polymer-Pt colloids and pure Pt colloids show a deeper brown color (Fig. S1). It can be seen from Fig. 1A that bare Pt NPs in Pt colloids are dispersed with an average size of 2.4 ± 0.5 nm (Fig. 1B), and aggregation can also be observed. Fig. S2 displays XRD patterns of bare Pt NPs. The characteristic diffraction peaks at 2θ of 39.7°, 46.2° and 67.5° are attributed to (111), (200), (220) crystal planes of face-centered cubic Pt phase (JCPDF 65-2868). The broadening of the diffraction peaks indicates the sizes of the Pt particles are in nanometer range, consistent with the results obtained from the TEM image. The inset of Fig. 1A displayed a *d* spacing of 0.228 nm, indexed well as the (111) plane of metallic Pt NPs.

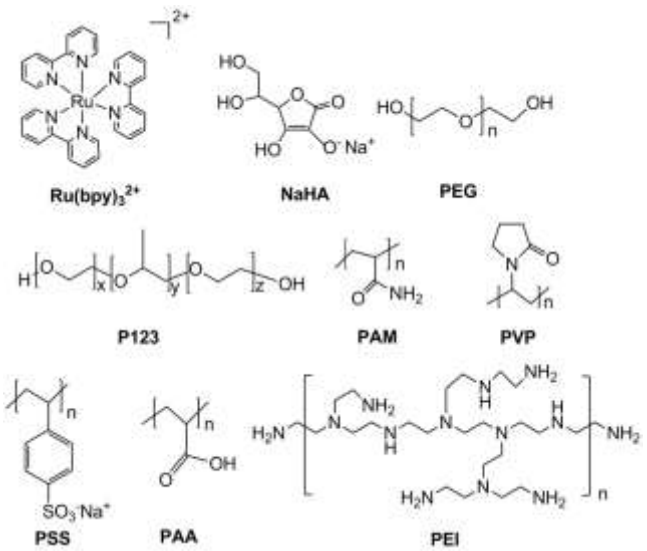

Scheme 2 Chemical structures of polymers used in this work

The morphology and average size of Pt colloids are almost no change with the addition of PEG (Fig. 1C and D), while the addition of P123 decreases the average size of Pt colloids to 2.0 ± 0.4 nm (Fig. 1F), along with agglomeration (Fig. 1E). It implies that PEG and P123 are not good stabilizers for Pt NPs,

because the interaction between the hydroxyl groups of non-ionic PEG or P123 and Pt NPs (Scheme 2) is too weak to completely inhibit the particle agglomeration. When PAM or PVP were used as stabilizers, the particle size of Pt becomes very small, with just about 1.5 nm (Fig. 1H and J). This is mainly because the acylamino groups in PAM or PVP easily adhere to the surface atoms of Pt NPs. As a result, it can reduce the surface free energy of Pt NPs and inhibit their growth and aggregation.[40] The PVP-Pt colloids show highly mono-dispersed Pt NPs without aggregation (Fig. 1I), while the PAM-Pt colloids provide ill-dispersed Pt NPs with a small amount of aggregation (Fig. 1G). In addition, the ionic polymers leads to a clear agglomeration of Pt NPs with an average particle size of ca. 2.0 nm, as shown in Fig. 1K-P, representing TEM images and particle-size distributions of Pt colloids modified by ionic polymers including PSS, PAA, and PEI. There is hardly difference in morphology, size, and dispersion of Pt NPs modified by these ionic polymers. It implies that PSS, PAA, PEI are not good stabilizers for Pt NPs. These results indicate that PVP is the best soluble polymer stabilizer for Pt NPs.

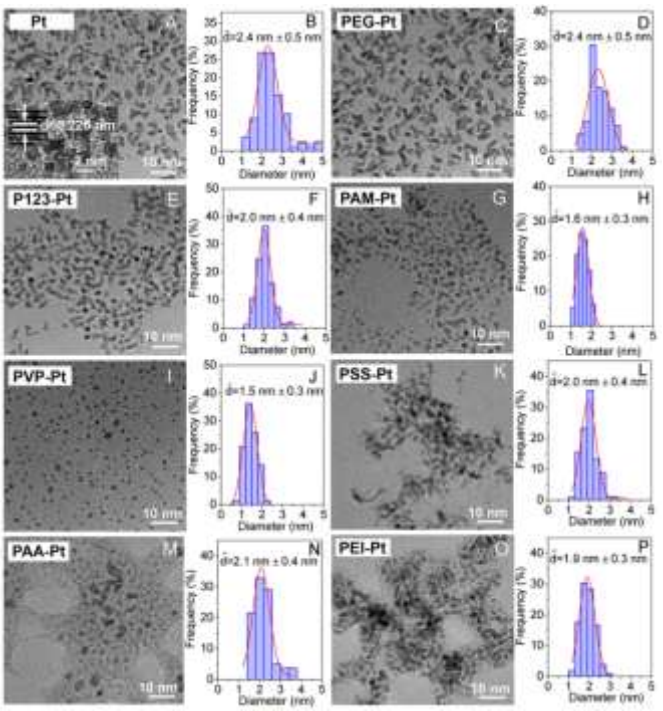

Fig. 1 HRTEM images, and particle-size distributions histograms of Pt, PEG-Pt, P123-Pt, PAM-Pt, PVP-Pt, PSS-Pt, PAA-Pt and PEI-Pt colloids.

These modified Pt NPs as hydrogen-evolving catalysts are used to assemble the artificial photosystem of SHF production with the $Ru(bpy)_3^{2+}$ photosensitizer, where no electron mediators are added beside the sacrificial reagent NaHA. The optimal pH value of the system is equal to 4.0, where the highest H_2 production rate is achieved (see Fig. 5). Fig. 2 shows the time course of hydrogen production at pH = 4 under visible light irradiation. No hydrogen evolution is discernable in the

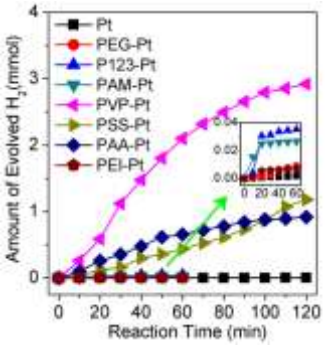

Fig. 2 Time course of hydrogen evolution under visible light irradiation ($\lambda \geq 420$ nm) of a mixed solution (150 ml) composed of $Ru(bpy)_3Cl_2$ (66.7μM), NaHA (50 mM), Pt (167 μM) and different polymers (8.35 mM) at initial pH 4.

system of bare Pt NPs as catalyst, implying no electron transfer between the photosensitizer (PS) and the hydrogen-evolving catalyst. It also can be seen that the PVP-Pt, PSS-Pt, and PAA-Pt systems are highly photoactive for H_2 evolution with vigorous bubbles of H_2 generating as soon as light irradiation starting, while the hydrogen evolution in other systems including PEG-Pt, PAM-Pt, P123-Pt, and PEI-Pt is very weak, even negligible. Control experiments indicate that $Ru(bpy)_3Cl_2$, NaHA, Pt and PVP (or PSS or PAA) were all essential for H_2 generation. The absence of any components gives rise to no hydrogen evolution (Fig. S3). Due to the poor stabilization for Pt NPs with PEG, P123 and PEI, not only Pt NPs are aggregate, but also the negatively-charged Pt NPs (-27.1 eV) and the cationic photosensitizer $Ru(bpy)_3^{2+}$ lead to the complex aggregations, which can be seen by naked eyes, accounting for their activity results.[41] Both of PAM and PVP are good stabilizers for Pt NPs, but PAM-Pt show little catalytic activity for hydrogen production, while PVP-Pt with high activity. It implies that the polymer (PAM) only stabilize Pt NPs, but can't assist the electron transfer between PS and catalyst. The O=C-N groups link with linear alkyl in PAM is neutral. However, PVP shows weak negatively-charged properties due to the inner O=C-N bond of pyrrolidinone inclined to $-N^+=C-O^-$ bond with N atom located inside and O atom located outside[42]. It can thus combine with positive charged $Ru(bpy)_3^{2+}$ to form the spatially-separated donor-acceptor complex by weak electrostatic force. The partial positive charge on the N atom behaved as electron acceptor and negative charge on the O atom behaved as electron donor.[43] Thus, PVP plays an important role as a bridge in the electron transfer process of photocatalytic hydrogen production. The same goes for PSS-Pt and PAA-Pt systems. It is also reasonable to believe that Pt NPs modified with polyanions and PVP can assemble with positively-charged $Ru(bpy)_3^{2+}$ by the electrostatic interaction to form a complex hybrid. Although, PSS and PAA can't stabilize Pt NPs, they can well assist the electron transfer from $Ru(bpy)_3^{2+}$ to Pt NPs. The comprehensive study will be discussed in section 3.4 later.

3.2. Size Effect of PVP-Pt_n NPs

PVP is chosen as the best modifier of Pt NPs for studying size effect of Pt NPs. PVP-Pt_n (where n is defined as Pt atom number) colloids with different sizes of Pt NPs were prepared by controlling NaOH concentration to optimize the photosystem. As seen from Table S1, the average diameter of Pt NPs decreases with increasing NaOH concentration. All the PVP-Pt_n colloidal solutions display a transparent, homogeneous and pale brown color (Fig. 3A) and show high stability. Fig. 3B-K showed their HRTEM images and corresponding size-distribution histograms. All particles were approximately spherical and monodisperse without aggregation. The size distribution of these particles is narrow, with an average diameter of 1.2 nm for PVP-Pt_{60} (Fig. 3B), 1.3 nm for PVP-Pt_{75} (Fig. 3D), 1.4 nm for PVP-Pt_{95} (Fig. 3F), 1.5 nm for PVP-Pt_{115} (Fig. 3H), and 2.0 nm for PVP-Pt_{276} (Fig. 3J), respectively.

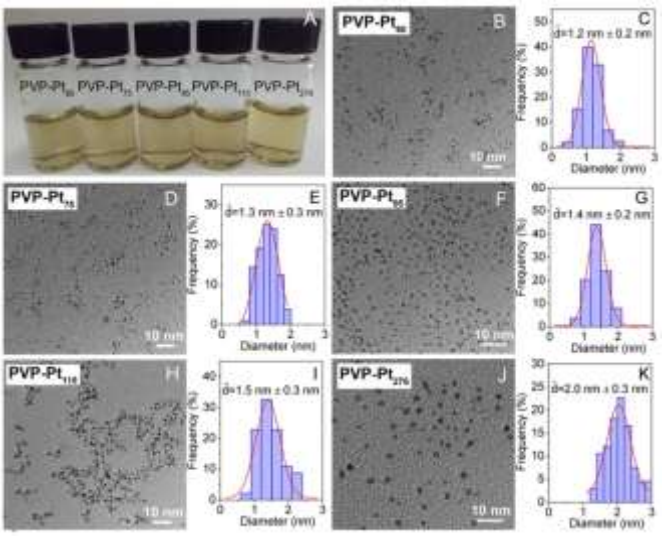

Fig. 3 Photographs, HRTEM images, and particle-size distributions histograms of PVP-Pt_{60}, PVP-Pt_{75}, PVP-Pt_{95}, PVP-Pt_{115}, and PVP-Pt_{276} colloids.

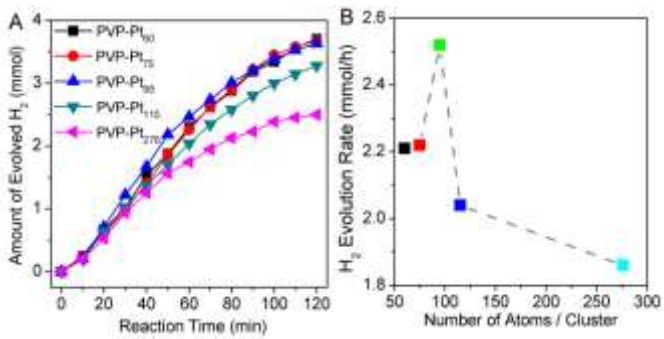

Fig. 4 (A) Time course of hydrogen evolution under visible light irradiation ($\lambda \geq 420$ nm) of a deaerated mixed aqueous solution (150 mL) containing $Ru(bpy)_3Cl_2$ (66.7 μM), NaHA (50 mM), PVP (8.35 mM) and Pt_n(167 μM, n=60, 75, 95, 115, 276) at initial pH 4. (B) Plots of initial hydrogen-evolution rates with size-selected Pt clusters as a function of cluster sizes. The hydrogen evolution rates were determined from the initial slopes of the time courses of hydrogen evolution in the first 30 min.

The size effect of the PVP-Pt_n colloids for the photocatalytic hydrogen evolution was evaluated under the same experimental conditions (using $Ru(bpy)_3^{2+}$ as a photosensitizer and NaHA as a sacrificial reagent at pH = 4.0). The time course of hydrogen evolution and the initial H_2 production rates versus cluster size are shown in Fig. 4A and B, respectively. With increasing size of PVP-Pt colloids, the H_2 production rate first increases and reaches a maximum at n = 95, along with a sharp decrease. The highest H_2 production rate is achieved up to 2.5 mmol/h in the $Ru(bpy)_3^{2+}$-PVP-Pt photosystem, and the optimal size of Pt NPs as H_2-evolving catalysts is equal to 1.4 nm (PVP-Pt_{95} colloids). The results are contributed synthetically from two aspects: (1) the smaller size of PVP-Pt_n catalysts, until the occurrence of quantum size effect,[44] the more amounts of explored surface Pt atoms; (2) larger size particles can receive more electrons.[45] The PVP-Pt_{95} exhibiting the highest hydrogen evolution rate was selected to be the H_2 evolving catalyst, abbreviated as PVP-Pt, in subsequent experiments.

3.3. Optimization of the H_2-Evolving Photosystems

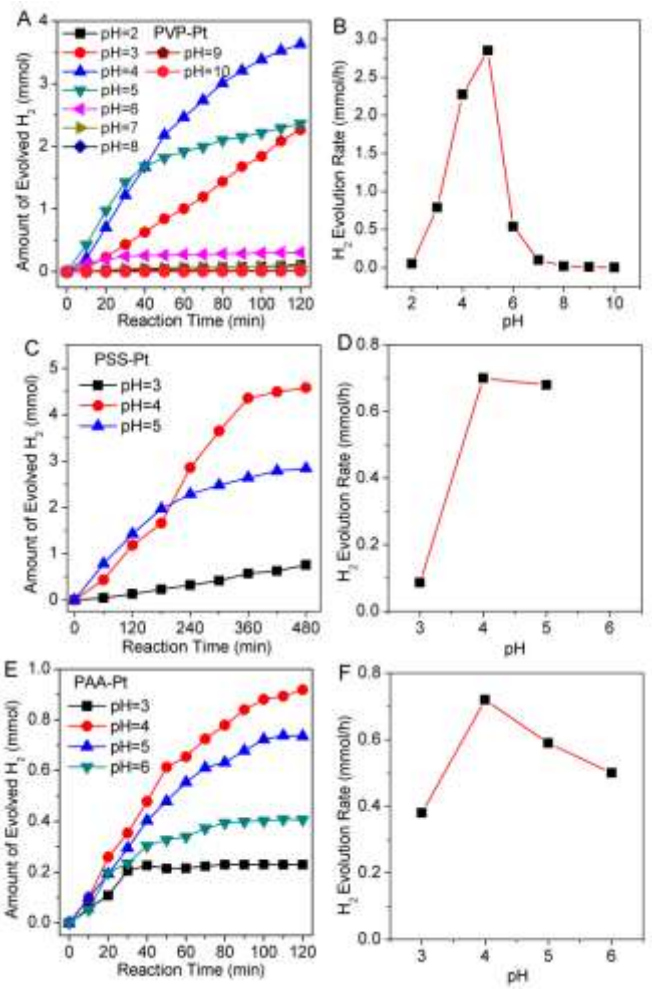

Fig. 5 Time course of hydrogen evolution with various pH values and initial rate of hydrogen generation as the function of pH under visible light irradiation ($\lambda \geq 420$ nm) of a deaerated mixed aqueous solution (150 mL) containing $Ru(bpy)_3Cl_2$ (66.7 μM), NaHA (50 mM), Pt (167 μM) and polymer (8.33 mM, PVP for A and B, PSS for C and D, PAA for E and F). The hydrogen evolution rates were

determined from the initial slopes of the time courses of hydrogen evolution in the first 30 min.

The pH influence is significant for the H_2-evolving photosystem, mainly owing to several factors including the redox potential of protons, the electrostatic properties of polymer-Pt colloids, and the chemical equilibrium of equilibrium of $H_2A \leftrightarrow H^+ + HA^-$.[46,47] Hydrogen evolution as a function of pH value is first examined and shown in Fig. 5. It can be seen that a large amount of H_2 is produced at pH = 3.0 to 5.0. The maximal yield of H_2 obtain at pH = 4.0, which is

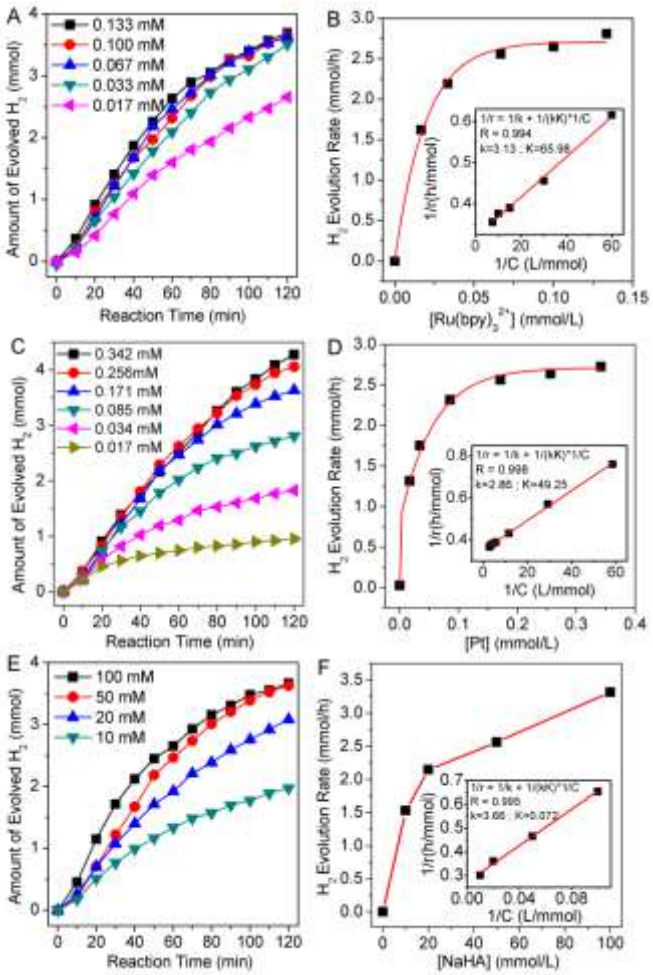

Fig. 6 Effects of $Ru(bpy)_3Cl_2$ (A), Pt (C) and NaHA (E) initial concentrations on H_2 production. Initial rate of hydrogen generation (r) versus $Ru(bpy)_3Cl_2$ (B), Pt (D), NaHA (F) initial concentration (c). The inserts show the fitting plot of 1/r versus 1/c. The hydrogen evolution rates were determined from the initial slopes of the time courses of hydrogen evolution in the first 30 min.

just the pK_{a1} value of the reaction of $H_2A \leftrightarrow H^+ + HA^-$, while H_2 production are only a little, even negligible below pH 3.0 and above pH 6.0 (Fig. 5 A). This is predominantly contributed from the repulsive interaction between positively-charged $Ru(bpy)_3^{2+}$ and positive-charged polymer-Pt colloids below pH 3.0 (see Fig. S4). Additionally, the equilibrium of $H_2A \leftrightarrow H^+ + HA^-$ shifts towards left and reduces the concentration of the electron donor HA^- below pH 4.0, consequently the significant decrease in H_2 evolution rate. As shown in Fig. S4, the zeta potentials of polymer-Pt colloids decrease from positive to negative with increasing pH value from 2 to 10. As pH increases, the decrease in proton concentration kinetically reduces the photoactivity. Therefore, the pK_{a1} value of the reaction is selected to be the value of pH of the $Ru(bpy)_3^{2+}$-Polymer-Pt artificial photosystem.

The effect of relative concentrations of $Ru(bpy)_3Cl_2$, Pt and NaHA on H_2 production was investigated. Fig. 6 shows the H_2 evolution as a function of reactant concentrations. As increasing the concentration of $Ru(bpy)_3Cl_2$ (Fig. 6A), the H_2 production rate increases rapidly and reached a maximal at $[Ru(bpy)_3Cl_2]$ = 66.7 μM. It is originated from the optical properties of the PS, which exhibits the maximal intensity of fluorescence emission at $[Ru(bpy)_3Cl_2]$ = 66.7 μM (Fig. S5). The high PS concentration results in self-quenching of the excited state, accounting for the photocatalytic activity. The initial H_2 evolution rate follows a Langmuir-type reaction model, which is generally applied to a kinetics analysis for heterogeneous gas-solid and liquid-solid systems[48], as a function of the concentration of $Ru(bpy)_3Cl_2$, where the rate constant of H_2 evolution and the adsorption constant of $Ru(bpy)_3Cl_2$ are 3.13 mmol h^{-1} and 65.98 L $mmol^{-1}$, respectively (Fig. 6B). Also, Pt (Fig. 6D), and NaHA (Fig. 6F) show the Langmuir-type reaction model with a H_2-evolution rate constant of k = 2.86 for Pt, 3.66 mmol h^{-1} for NaHA and an adsorption constant of K = 49.25 for Pt, 0.072 L $mmol^{-1}$ for NaHA. When the concentration of Pt and NaHA is, respectively, higher than [Pt] =0.171 mM (Fig. 6C) and [NaHA] = 50 mM (Fig. 6E), no more hydrogen is evolved for the first two illuminated hours. According to the adsorption constant obtained, it can be concluded that the reaction is kinetically controlled by the Pt adsorption, implying the critical role of the electron transfer between PS and Pt catalyst in the hydrogen evolution. Note that the substitution of NaHA by other electron donors, such as sodium ethylenediaminetetraacetic (EDTA-2Na) and triethanolamine (TEOA), often used in photoreactions at their optimal pH, resulted in trace amount of H_2 production (Fig. S6), indicating NaHA is the most effective electron donor for our artificial photosystem.

Interestingly, polymer doesn't follow the same kinetic model of H_2 evolution as Pt and PS. As shown in Fig. 7, an optimal hydrogen evolution rate of ca. 2.50 mmol h^{-1} is achieved at [PVP] = 0.667 mM (Fig. 7A and B). The optimal mole ratio of PS/PVP/surface Pt atoms is calculated to be 1:10:1.7 (see Table S2 in the Supporting Information for details). Addition of more PVP leads to a slight decrease in hydrogen evolution rate. Also, the artificial photosystems of $Ru(bpy)_3^{2+}$-PSS-Pt and $Ru(bpy)_3^{2+}$-PAA-Pt show the same reaction models as PVP. An optimal addition is achieved to be 0.167 mM for PSS and 1.33 mM for PAA (Fig. 7C-F), where the optimal mole ratio of PS/polymers/surface Pt atoms is calculated to be about 1:2.5:1.3 and 1:20:1.3, respectively (see Table S2 in the Supporting Information for details). A sharp decrease in hydrogen evolution rate occurs above the concentrations of PSS

and PAA. Obviously, more amounts of PVP, PSS and PAA are all deleterious to the hydrogen production. This is because surplus polymer can adsorb and wrap $Ru(bpy)_3^{2+}$, resulting to decreased contact between the negative-charged NaHA and $Ru(bpy)_3^{2+}$, Consequently, the intermolecular electron transfer is hindered. The decreasing trend follows the order of PSS > PAA > PVP, in consistence with their negatively charged properties (see Fig. S4). We can see that these polymers don't follow the Langmuir-type reaction model. It implies that the polymers function an important role in the PS-Polymer-Pt artificial photosystems, which will be discussed in depth later.

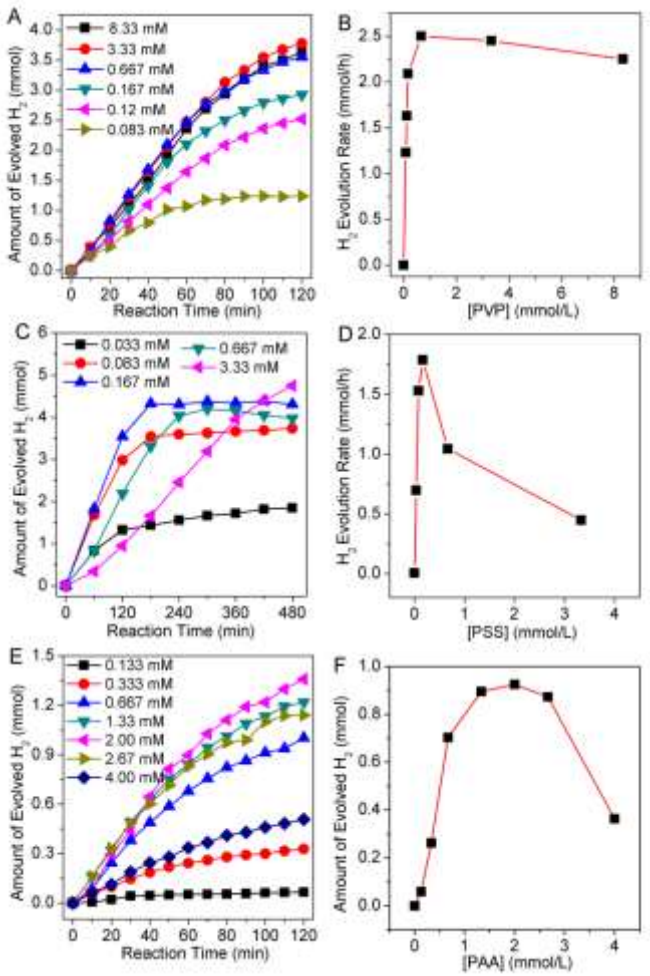

Fig. 7 Effects of PVP (A), PSS (C) and PAA (E) initial concentrations on H_2 production. Initial rate of hydrogen generation versus PVP (B), PSS (D) and PAA (F) initial concentration. The hydrogen evolution rates were determined from the initial slopes of the time courses of hydrogen evolution in the first 30 min.

Under the conditions of pH = 4, $[Ru(bpy)_3Cl_2]$ = 66.7 μM, [Pt] =0.171 mM, [PVP] = 0.667 mM , and [NaHA] = 50 mM, the optimal apparent quantum efficiency of hydrogen production can be obtained under different-wavelength light irradiation. Fig. 8 depicts the spectrum action of quantum efficiencies. The H_2 production matches basically with the UV-vis absorption spectrum of $Ru(bpy)_3Cl_2$-PVP-Pt in aqueous solution. The distinguished large quantum efficiency of 12.8% is obtained at 450 nm, it is corresponding to the maximum absorption of $Ru(bpy)_3Cl_2$-PVP-Pt in the visible light region. At 475 nm, the quantum efficiency is still as high as 12.3%. Above 475 nm wavelength, the quantum efficiency decreases considerably due to a decrease in absorption of $Ru(bpy)_3Cl_2$-PVP-Pt.

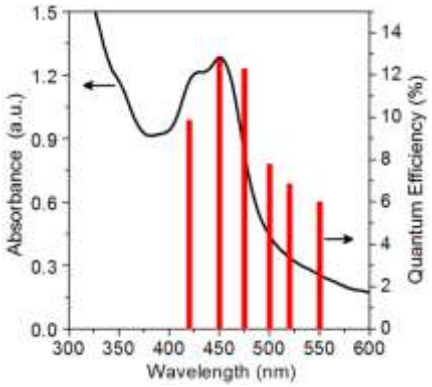

Fig. 8 UV-vis absorption spectrum of $Ru(bpy)_3Cl_2$-PVP-Pt and the quantum efficiencies of hydrogen evolution under photons with different wavelengths over the $Ru(bpy)_3Cl_2$/PVP-Pt/NaHA system. Conditions: $[Ru(bpy)_3Cl_2]$ = 66.7 μM, [Pt] =0.171 mM, [PVP] = 0.667 mM , and [NaHA] = 50 mM, pH = 4.0.

3.4. Understanding of Intermolecular Interactions of $Ru(bpy)_3^{2+}$-Polymer-Pt

Without an additional electron relay, hydrogen gas can be indeed produced in the $Ru(bpy)_3^{2+}$-polyanion-Pt system using NaHA as an electron donor under visible light irradiation. The kinetic analysis mentioned above indicates that the H_2 evolution proceeds in a heterogeneous manner in the self-assembled photosystem, where $Ru(bpy)_3Cl_2$, polymers, and Pt NPs are bonded to form a spatially-separated donor-acceptor complex $Ru(bpy)_3^{2+}$-polymer-Pt. Although the effect of PVP on the absorption of $Ru(bpy)_3^{2+}$ is indiscernible due to the weak electrostatic interaction (Fig. S7A). Also, adding PVP-Pt colloids into $Ru(bpy)_3Cl_2$ solution doesn't change the absorption. It shows only a simple plus of the UV-Vis spectrum of PVP-Pt with $Ru(bpy)_3^{2+}$. However, after adding PSS and PAA, a slight red shift is discernable for the absorption feature at 453 nm belonging to metal to ligand charge transfer (MLCT) band of $Ru(bpy)_3^{2+}$ (Fig. S7D, G)[49]. Moreover, the degree of red shift is constant with increasing concentrations of the polyanions, indicating no concentration dependence of the shift of MLCT bands of $Ru(bpy)_3Cl_2$. The result indicates that hybrids are formed in these conditions. These results further indicate that the polyanions (PSS and PAA) are strongly bound to $Ru(bpy)_3^{2+}$ to form the self-assembled $Ru(bpy)_3^{2+}$-polymer hybrids by electrostatic interaction[50].

To further gain insight into the non-covalent interaction at molecular lever, fluorescence spectroscopy is applied to study the artificial photosystem. Fig. 9 shows the relative intensity and lifetime of the 610 nm emission as a function of polymer or quencher concentration. $Ru(bpy)_3^{2+}$ presents a significantly synchronous increase in intensity and lifetime of the 610 nm

emission with increasing PVP concentration (Fig. 9A, Fig. S8A, B). It implies that PVP does affect the triplet excited state of $*Ru(bpy)_3^{2+}$ due to the non-covalent interaction. The polymer PVP not only enables $*Ru(bpy)_3^{2+}$ more stable, but also enhances the intensity of fluorescence emission, reducing the energy loss. Also, addition of PSS and PAA induces a slight red shift of the emission maxima of $*Ru(bpy)_3^{2+}$, consistent with the red shift in the lowest energy MLCT absorption of $Ru(bpy)_3^{2+}$ (see Fig. S8 E, I). Moreover, they significantly increase the 610 nm emission of $*Ru(bpy)_3^{2+}$ (Fig. S8 E, I). As shown in Fig. 9C, E and Fig. S8 E, I, the intensity and lifetime are increasing with the concentration of PSS and PAA, indicating the strong stabilization for the excited state $*Ru(bpy)_3^{2+}$ to attain relatively long-lived charge separation. This is mainly because the self-assembled $Ru(bpy)_3^{2+}$-polymer hybrids can decrease the rate of deactivation via the intermolecular nonradiative paths.[51] The increasing trend of fluorescence intensity and lifetime follows the order of PSS > PAA > PVP, in consistence with electrostatic attraction between the polymer and $Ru(bpy)_3^{2+}$. The stronger the attraction is, the easier the $Ru(bpy)_3^{2+}$-polymer hybrid forms. When the concentration of PSS reaches 1.0 mmol/L, addition of more amounts of PSS leads to no change of fluorescence intensity and lifetime of $*Ru(bpy)_3^{2+}$ (Fig. 9C). Meanwhile, we believe that the change trend of relative fluorescence intensity and lifetime of $*Ru(bpy)_3^{2+}$ as increasing the concentration of PVP or PAA will just be similar to PSS. The maximal amount of PVP and PAA needed to form $*Ru(bpy)_3^{2+}$ with longest lifetime will be larger than 8 mmol/L and 2.0 mmol/L, respectively. Therefore, adding appropriate amount of polymer can increase the intensity and lifetime of $*Ru(bpy)_3^{2+}$. But, excessive polymer is unhelpful for increasing the fluorescence intensity and lifetime. On the contrary, they reduce the probability of collision between the NaHA and $Ru(bpy)_3^{2+}$, resulting in decrease of electron transfer. It is consistent with the photocatalytic activity results.

However, adding bare Pt colloids to the $Ru(bpy)_3Cl_2$/PVP solution significantly quenches the 610 nm emission (Fig. 9B, Fig. S8C). The fluorescence intensity is decreased linearly with increasing Pt concentration, but the fluorescence lifetime of $*Ru(bpy)_3^{2+}$ in the system shows no change (Fig. 9B, Fig. S8D). On the basis of Förster dipole-dipole non-radiative energy-transfer theory, a resonance energy transfer (RET) can occur whenever the emission spectrum of a fluorophore, called the donor, overlaps with the absorption spectrum of another molecule (see Fig. S7), called the acceptor and the distance between them is about 10 - 100 Å.[52] Apparently, an intermolecular RET occurs from $*Ru(bpy)_3^{2+}$-PVP to Pt NPs. The linear fits of the intensity quenching (Fig. 9B) yield a Stern-Volmer (SV) constant, K_{sv}, of 4332 M^{-1}, and the relationship $K_{sv} = \kappa_{ENT}\tau_D$, (where $\tau_D = 545.0$ ns , is the emission lifetime of $*Ru(bpy)_3^{2+}$-PVP in absence of Pt) yields an energy transfer rate constant, κ_{ENT}, of 8.0×10^9 M^{-1} S^{-1}. Meanwhile, the addition of Pt colloids into the PS/PSS and PS/PAA solution makes the 610 emission reduced drastically, whereas the lifetime shows no change (Fig. 9D and F). The result clearly indicates the occurrence of RET between $*Ru(bpy)_3^{2+}$-polymer and Pt NPs. The energy transfer rate constant, κ_{ENT}, is 9.0×10^9 M^{-1} S^{-1} for PSS and 24.8×10^9 M^{-1} S^{-1} for PAA. These quenching process follow a static mechanism. It indicates that Pt colloids are adsorbed strongly into the $Ru(bpy)_3^{2+}$-polymer complexes. Furthermore, according to Förster theory, the rate of RET depends strongly on donor-to-acceptor distance (r), and is proportional to r^{-6}.[53] The $Ru(bpy)_3^{2+}$-to-Pt distance in the $Ru(bpy)_3^{2+}$-polymer-Pt self-assembly follows the decreased order of PAA<<PSS<PVP, corresponding to the hydrogen evolution rate.

In a word, $Ru(bpy)_3^{2+}$ and polyanions/PVP can be self-assembled by strong electrostatic interaction to form a complex hybrid. And Pt colloids are adsorbed strongly into the $Ru(bpy)_3^{2+}$-polymer by non-covalent intermolecular interaction to form the spatially-separated donor-acceptor complex $Ru(bpy)_3^{2+}$-Polymer-Pt. In these process, polymers play several important roles: (1) polymers can stabilize excited state $*Ru(bpy)_3^{2+}$ with long-lived charge separation; (2) polymers act as bridges to closely connect $Ru(bpy)_3^{2+}$ with Pt, consequently accelerating the energy transfer from PS to catalyst.

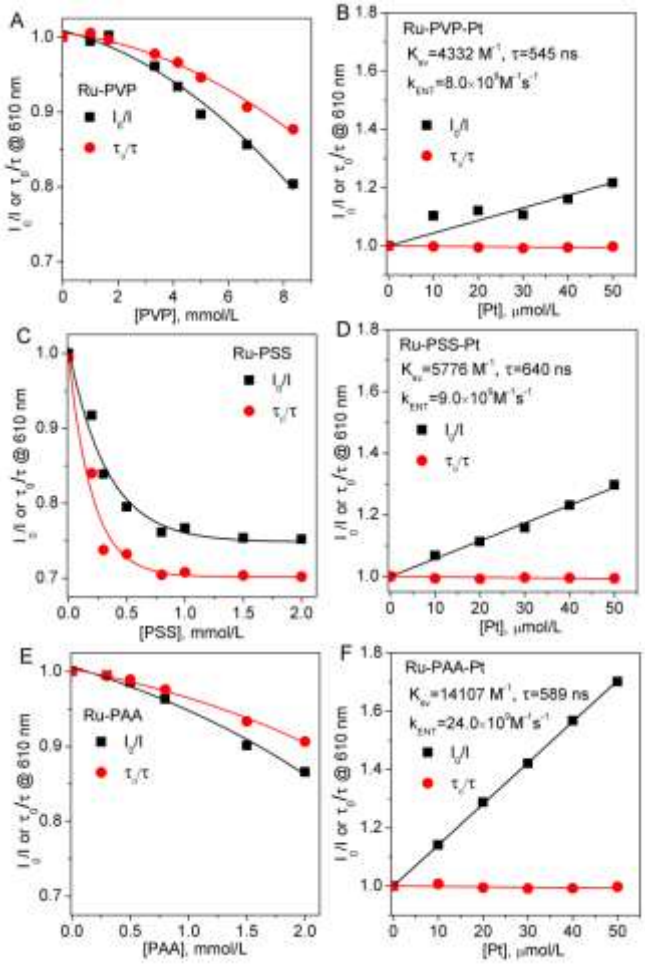

Fig. 9 Change (A, C, E) of the relative fluorescence intensity and lifetime of $Ru(bpy)_3Cl_2$ (2.5×10^{-5} M) solution with increasing concentrations of polymer at pH = 4.0. Stern–Volmer plots (B, D, F) of the fluorescence quenching and lifetime quenching of

$Ru(bpy)_3Cl_2$ (2.5×10^{-5} M) by Pt colloids in the presence of anionic polymers (8.0×10^{-4} M) at pH = 4.0.

3.5. Mechanism of Photocatalytic Hydrogen Production of NaHA-$Ru(bpy)_3^{2+}$-Polymer-Pt Systems

To explore the details of photocatalytic mechanism, we performed the steady-state photolysis experiments. 50 ns laser excitation of $Ru(bpy)_3^{2+}$ in aqueous solution gives rise to a negative absorption band from λ = 400 to 500 nm corresponding to the depopulation of the MLCT ground-state absorption band of PS and a positive absorption feature at ca. 370 nm, which is a characteristic of PS*, with a decay lifetime of about 600 ns (Fig. S9). It has enough time to quench PS* with HA^-. The reductively quenching is permissible thermodynamically, because the first reduction potential of the triplet excited state PS* is estimated to be +0.84 V vs SCE ($/Ru^{II}*/Ru^{I}$)[54], larger than the potential (+0.28 V vs SCE) of the couple $HA^{\bullet}/HA^-$[55]. The reductively quenching processes were studied by time-resolved fluorescence spectroscopies, as shown in Fig. 10 and Fig. S10. The linear fits of the intensity quenching (Fig. 10A) yield a Stern-Volmer (SV) constant, K_{sv}, of 39.5 M^{-1}, for the free $Ru(bpy)_3^{2+}$ system without any polymers, and the relationship $K_{sv} = \kappa_q\tau_0$, (where $\tau_0 = 554.0$ ns, is the emission lifetime of $*Ru(bpy)_3^{2+}$) yields a quenching rate constant, κ_q, of 7.13×10^7 M^{-1} S^{-1}. Lifetime quenching (LQ) by NaHA is calculated to be K_{sv}= 36.8 M^{-1} and κ_q = 6.7×10^7 M^{-1} S^{-1} (Fig. 10B), similar to the intensity quenching rate constant, indicating that the quenching of $*Ru(bpy)_3^{2+}$ by NaHA by a dynamic mechanism of electron transfer from NaHA to $*Ru(bpy)_3^{2+}$. The addition of polymers decreases both SV and LQ constants (Fig. 10), which is a further indicative of the stabilization of polyanions to $*Ru(bpy)_3^{2+}$, following the decreased order of PVP (35.7 and 24.4 M^{-1} for SV and LQ constants, respectively; $\tau_0 = 556.0$ ns, is the emission lifetime of $*Ru(bpy)_3^{2+}$-PVP) > PAA (25.7 and 18.0 M^{-1} for SV and LQ constants, respectively; $\tau_0 = 569.0$ ns, is the emission lifetime of $*Ru(bpy)_3^{2+}$-PAA) > PSS (7.60 and 2.6 M^{-1} for SV and LQ constants, respectively; $\tau_0 = 684.0$ ns, is the emission lifetime of $*Ru(bpy)_3^{2+}$-PSS at pH =4.0).

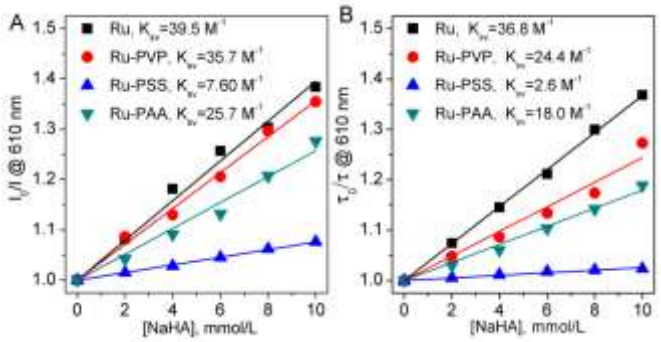

Fig. 10 Stern–Volmer plots of the fluorescence quenching (A) and lifetime quenching (B) of $Ru(bpy)_3^{2+}$ or $Ru(bpy)_3^{2+}$-Polymer by NaHA. Condition: $Ru(bpy)_3^{2+}$ (2.5×10^{-5} M), polymer (8.0×10^{-4} M) at pH=4.

The quenching product of $*Ru(bpy)_3^{2+}$ by NaHA was studied by the transient absorption spectra of the systems composing of NaHA-$Ru(bpy)_3^{2+}$ (Fig. 11A, B) and NaHA-$Ru(bpy)_3^{2+}$-PVP-Pt (Fig. 11C). After 50 ns laser excitation of a deaerated aqueous solution at pH =4.0 containing $Ru(bpy)_3^{2+}$ (2.5×10^{-5} M) and NaHA (0.05 M), two transient absorption bands appear at λ = 310-400 and 470-550 nm (Fig. 12A). The new band with a maximum at 510 nm is a characteristic of $[Ru(bpy)_3]^+$. [56] It is growing concomitantly with the decrease of the PS* absorption band at 370 nm, confirming the electron transfer from HA^- to PS*. The generation of $[Ru(bpy)_3]^+$ obeys pseudo-first-order kinetics with a lifetime of 264 ns and a rate constant of 3.1×10^7 M^{-1} S^{-1} (Fig. S11). The decay of the entire transient absorption spectra of the systems composed of NaHA-$Ru(bpy)_3^{2+}$ (Fig. 11B) and NaHA-$Ru(bpy)_3^{2+}$-PVP-Pt (Fig. 11C) occurs in few hundred of microseconds, corresponding to the return of PS^- to the ground state PS, respectively, with a pseudo-first-order rate constant of 1.5×10^4 and 2.3×10^4 S^{-1}. The rate constant of $[Ru(bpy)_3]^+$ decay in NaHA-$Ru(bpy)_3^{2+}$-PSS-Pt and NaHA-$Ru(bpy)_3^{2+}$-PAA-Pt system is 2.0×10^4 S^{-1} and 2.3×10^4 S^{-1}, respectively (Fig. S12A). Evidently, addition of the polyanion-Pt considerably improves the return of PS^- to PS, releasing electron to Pt catalyst, where H^+ is reduced into hydrogen gas.

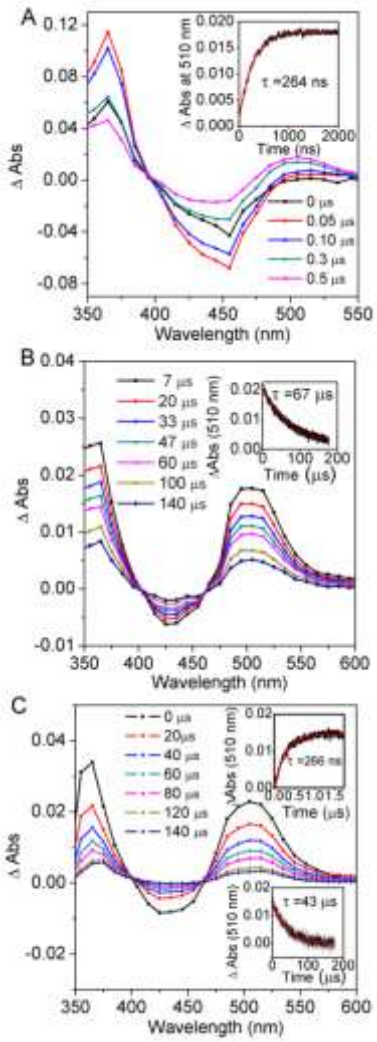

Fig. 11 Transient absorption spectra after laser excitation at λ = 450 nm of a deaerated aqueous solution containing $Ru(bpy)_3^{2+}$ (2.5×10^{-5} M), NaHA (0.05 M) at pH 4.0 (path length=1 cm) within the time ranges 0–500 ns (A) and 700 ns–167 μs (B). Insets of A) and B) are the growth time profile and the decay time profile of the absorbance at λ = 510 nm arising from $Ru(bpy)_3^{+}$ aqueous solution, respectively. (C) Transient absorption spectra after laser excitation of a deaerated aqueous solution containing $Ru(bpy)_3^{2+}$ ($^{2.5\times10^{-5}}$M), NaHA (0.05 M) PVP ($^{8.0\times10^{-4}}$M), Pt ($^{2.0\times10^{-4}}$M M) at pH 4.0 (path length=1 cm) within the time range 0 – 160 μs. Insets of (up) and (down) are the growth time profile and the decay time profile of the absorbance at λ = 510 nm arising from $Ru(bpy)_3^{+}$ present in this aqueous solution, respectively.

In order to make the role of polymers in the electron transfer process clear, time profiles of the absorption at 510 nm in the presence of $Ru(bpy)_3^{2+}$ and polymers was studied. As shown in Fig. S12B, addition of polymers results in faster decay. It implies that electron can transfer from $Ru(bpy)_3^{+}$ to polymers. Unluckily, the laser photolysis experiments can't obtain any evidences for the formed radical of polymer. The polymer-Pt systems might undergo a complex mechanism than the simple back electron transfer between PS^- and $HA^{\bullet}$. We believe that some other reactions involve the return of PS^- to PS for addition of polyanion-Pt catalysts. However, hydrogen can evolve efficiently in the $Ru(bpy)_3^{2+}$-polymer-Pt systems by adding several polymers including PVP, PSS, and PAA, indicating the smooth electron transfer between PS^- and the hydrogen-evolving catalyst Pt NPs. While the fact that the hydrogen evolution is inefficient, even negligible in the bare Pt system, indicates the severely blocking of electron transfer between PS^- and the hydrogen-evolving catalyst. It is certain that without addition of polymers into the artificial photosystem, no electron transfer occurs between PS^- and the hydrogen-evolving catalyst Pt NPs. A reasonable concept of electronic bridge is proposed to well explain the role of polymers used in hydrogen evolution. Electrons can be transferred from PS to catalyst in virtue of them by the mechanism of electron-electron self-exchange between anionic groups.[57,58] Therefore, the photocatalytic H_2 evolution of the NaHA-$Ru(bpy)_3^{2+}$-polymer-Pt system follows the mechanism shown in Scheme 3. The reaction process is summarized as follows: 1) Upon photo-excitation of $Ru(bpy)_3^{2+}$-polymer-Pt in the present of NaHA, the exited state $^*Ru(bpy)_3^{2+}$ moiety is formed, and it is quenched by HA^- to produce the reductive state $Ru(bpy)_3^{+}$ moiety; 2) Electrons may be transferred from the $Ru(bpy)_3^{+}$ moiety to the Pt moiety through the electron-electron exchange of polymers; 3) Protons are reduced to H_2 on the surface of Pt NPs.

4. Conclusions

$Ru(bpy)_3Cl_2$ and polymer-Pt were self-assembled *in situ* to form a spatially separated donor-acceptor complex by the non-covalent interaction. The quasi-supermolecular complex showed high-efficiency visible-light photocatalytic hydrogen evolution in the presence of NaHA as a sacrificial electron donor without adding a conventional molecular type of electron mediator. The maximum amount of hydrogen production was achieved when the concentrations of $Ru(bpy)_3Cl_2$, PVP (or PSS or PAA), Pt and NaHA were fixed at 66.7 μM, 0.667 mM (or 0.167 mM or1.33 mM), 0.171 mM and 50 mM, respectively. Under the optimized conditions, the hydrogen evolution takes place with a distinguished large apparent quantum efficiency of 12.8 %. According to the results of nanosecond transient absorption and time-resolved fluorescence spectroscopies, a mechanism of electron transport via a polymeric wire bridging PS and Pt was proposed for the artificial $Ru(bpy)_3^{2+}$-polymer-Pt photosystems. The study provides a comprehensive insight into the role of polymers in the artificial photosystems for hydrogen production.

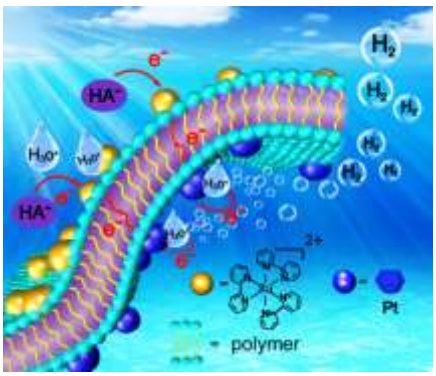

Scheme 3 Proposed catalytic mechanism for the light-driven H_2 evolution

Acknowledgements

This work was financially supported by the NSFC (Grants Nos. 21173044, 21373051 and U1305242), the Program for New Century Excellent Talents in Fujian Province University (JA14029), and the Program for Qishan Scholar of Fuzhou University. Long thanks Professor Li-Zhu Wu and Dr. Zhi-Jun Li for their assistance to the photophysical experiments.

Abbreviations

$Ru(bpy)_3^{2+}$ or Ru, tris (2, 2'-bipyridyl) ruthenium (II) chloride; PS, photosensitizer; NaHA, sodium ascorbate; NPs, nanoparticles; PAA, poly (acrylic acid); PAM, polyacrylamide; PEG, polythylene glycol; PVP, polyvinylpyrrolidone; P123, poly (ethylene glycol)-block-poly (propylene plycol)-block-poly (ethylene glycol) PSS, poly (sodium 4-styrenesulfonate); PEI, poly(ethyleneimine); $QuPh^+$-NA, 2-phenyl-4-(1-naphthyl) quinolinium ion; Acr^+-Mes, 9-mesityl-10-methylacridinium ion.

Notes and references

State Key Laboratory of Photocatalysis on Energy and Environment, School of Chemistry, Fuzhou University, Fuzhou 350116, P. R. China Tel: +86-591-83779251; Email: jllong@fzu.edu.cn ; xwang@fzu.edu.cn

† Electronic Supplementary Information (ESI) available: [details of any supplementary information available should be included here]. See DOI: 10.1039/b000000x/

1. J. M. Lehn and J. P. Sauvage, *Nouveau Journal De Chimie-New Journal of Chemistry*, 1977, **1**, 449-451.
2. J. Kiwi and M. Gratzel, *Nature*, 1979, **281**, 657-658.
3. I. Okura and N. Kim-Thuan, *Journal of Molecular Catalysis*, 1979, **5**, 311-314.
4. A. Magnuson, M. Anderlund, O. Johansson, P. Lindblad, R. Lomoth, T. Polivka, S. Ott, K. Stensjö, S. Styring, V. Sundström and L. Hammarström, *Accounts of Chemical Research*, 2009, **42**, 1899-1909.
5. A. Kudo and Y. Miseki, *Chemical Society Reviews*, 2009, **38**, 253-278.
6. W. T. Eckenhoff and R. Eisenberg, *Dalton Transactions*, 2012, **41**, 13004-13021.
7. F. Wen and C. Li, *Accounts of chemical research*, 2013, **46**, 2355-2364.
8. S. Berardi, S. Drouet, L. Francas, C. Gimbert-Surinach, M. Guttentag, C. Richmond, T. Stoll and A. Llobet, *Chemical Society Reviews*, 2014, **43**, 7501-7519.
9. L.-Z. Wu, B. Chen, Z.-J. Li and C.-H. Tung, *Accounts of chemical research*, 2014, **47**, 2177-2185.
10. T. Hisatomi, J. Kubota and K. Domen, *Chemical Society Reviews*, 2014, **43**, 7520-7535.
11. N. Mourtzis, P. C. Carballada, M. Felici, R. J. M. Nolte, R. M. Williams, L. de Cola and M. C. Feiters, *Physical Chemistry Chemical Physics*, 2011, **13**, 7903-7909.
12. P. Du, J. Schneider, P. Jarosz and R. Eisenberg, *Journal of the American Chemical Society*, 2006, **128**, 7726-7727.
13. H. Kotani, K. Ohkubo, Y. Takai and S. Fukuzumi, *The Journal of Physical Chemistry B*, 2006, **110**, 24047-24053.
14. Y. Amao, Y. Maki and Y. Fuchino, *The Journal of Physical Chemistry C*, 2009, **113**, 16811-16815.
15. H. Zhu, N. Song, H. Lv, C. L. Hill and T. Lian, *Journal of the American Chemical Society*, 2012, **134**, 11701-11708.
16. P. Keller and A. Moradpour, *Journal of the American Chemical Society*, 1980, **102**, 7193-7196.
17. S. Fukuzumi, *Physical Chemistry Chemical Physics*, 2008, **10**, 2283-2297.
18. P. Zhang, M. Wang, C. Li, X. Li, J. Dong and L. Sun, *Chemical Communications*, 2010, **46**, 8806-8808.
19. S. Losse, J. G. Vos and S. Rau, *Coordination Chemistry Reviews*, 2010, **254**, 2492-2504.
20. W. R. McNamara, Z. Han, P. J. Alperin, W. W. Brennessel, P. L. Holland and R. Eisenberg, *Journal of the American Chemical Society*, 2011, **133**, 15368-15371.
21. W. R. McNamara, Z. Han, C.-J. M. Yin, W. W. Brennessel, P. L. Holland and R. Eisenberg, *Proceedings of the National Academy of Sciences*, 2012, **109**, 15594-15599.
22. M. Natali, A. Luisa, E. Iengo and F. Scandola, *Chemical Communications*, 2014, **50**, 1842-1844.
23. W. Zhang, J. Hong, J. Zheng, Z. Huang, J. Zhou and R. Xu, *Journal of the American Chemical Society*, 2011, **133**, 20680-20683.
24. Z. Han, F. Qiu, R. Eisenberg, P. L. Holland and T. D. Krauss, *Science*, 2012, **338**, 1321-1324.
25. Z. Han, W. R. McNamara, M.-S. Eum, P. L. Holland and R. Eisenberg, *Angewandte Chemie International Edition*, 2012, **51**, 1667-1670.
26. M. A. Gross, A. Reynal, J. R. Durrant and E. Reisner, *Journal of the American Chemical Society*, 2013, **136**, 356-366.
27. F. Wang, W.-G. Wang, H.-Y. Wang, G. Si, C.-H. Tung and L.-Z. Wu, *ACS Catalysis*, 2012, **2**, 407-416.
28. L. L. Tinker, N. D. McDaniel, P. N. Curtin, C. K. Smith, M. J. Ireland and S. Bernhard, *Chemistry – A European Journal*, 2007, **13**, 8726-8732.
29. H. Kotani, T. Ono, K. Ohkubo and S. Fukuzumi, *Physical Chemistry Chemical Physics*, 2007, **9**, 1487-1492.
30. Y. Yamada, T. Miyahigashi, H. Kotani, K. Ohkubo and S. Fukuzumi, *Journal of the American Chemical Society*, 2011, **133**, 16136-16145.
31. W.-G. Wang, F. Wang, H.-Y. Wang, G. Si, C.-H. Tung and L.-Z. Wu, *Chemistry – An Asian Journal*, 2010, **5**, 1796-1803.
32. T. A. White, S. L. H. Higgins, S. M. Arachchige and K. J. Brewer, *Angewandte Chemie*, 2011, **123**, 12417-12421.
33. G. Ajayakumar, M. Kobayashi, S. Masaoka and K. Sakai, *Dalton Transactions*, 2011, **40**, 3955-3966.
34. M. Zhu, M. Han, Y. Du, P. Yang and X. Wang, *Dyes and Pigments*, 2010, **86**, 81-86.
35. M. Zhu, Y. Lu, Y. Du, J. Li, X. Wang and P. Yang, *International Journal of Hydrogen Energy*, 2011, **36**, 4298-4304.
36. M. Zhu, Y. Dong, Y. Du, Z. Mou, J. Liu, P. Yang and X. Wang, *Chemistry – A European Journal*, 2012, **18**, 4367-4374.
37. Y. Yamada, T. Miyahigashi, H. Kotani, K. Ohkubo and S. Fukuzumi, *Energy & Environmental Science*, 2012, **5**, 6111-6118.
38. W. Yu, W. Tu and H. Liu, *Langmuir*, 1998, **15**, 6-9.
39. Y. Sun and Y. Xia, *Science*, 2002, **298**, 2176-2179.
40. J.-F. Zhu and Y.-J. Zhu, *The Journal of Physical Chemistry B*, 2006, **110**, 8593-8597.
41. K. G. Thomas and P. V. Kamat, *Accounts of Chemical Research*, 2003, **36**, 888-898.
42. X. Sui, Y. Liu, C. Shao, Y. Liu and C. Xu, *Chemical Physics Letters*, 2006, **424**, 340-344.
43. R. M. Moriarty and J. M. Kliegman, *Tetrahedron Letters*, 1966, **7**, 891-896.
44. J. Kiwi and M. Graetzel, *Journal of the American Chemical Society*, 1979, **101**, 7214-7217.

45. N. Toshima, M. Kuriyama, Y. Yamada and H. Hirai, *Chemistry Letters*, 1981, 793-796.
46. F. Wang, W.-G. Wang, X.-J. Wang, H.-Y. Wang, C.-H. Tung and L.-Z. Wu, *Angewandte Chemie International Edition*, 2011, **50**, 3193-3197.
47. E. G. Ball, *Journal of Biological Chemistry*, 1937, **118**, 219-239.
48. X. Fu, J. Long, X. Wang, D. Y. Leung, Z. Ding, L. Wu, Z. Zhang, Z. Li and X. Fu, *International Journal of Hydrogen Energy*, 2008, **33**, 6484-6491.
49. J. L. Colon, C. Y. Yang, A. Clearfield and C. R. Martin, *The Journal of Physical Chemistry*, 1988, **92**, 5777-5781.
50. D. Meisel, M. S. Matheson and J. Rabani, *Journal of the American Chemical Society*, 1978, **100**, 117-122.
51. W. Dressick, J. Cline, J. N. Demas and B. DeGraff, *Journal of the American Chemical Society*, 1986, **108**, 7567-7574.
52. Y. Xu, D. W. Piston and C. H. Johnson, *Proceedings of the National Academy of Sciences*, 1999, **96**, 151-156.
53. W.-B. Wu, M.-L. Wang, Y.-M. Sun, W. Huang, Y.-P. Cui and C.-X. Xu, *Journal of Physics and Chemistry of Solids*, 2008, **69**, 76-82.
54. C. Creutz, B. S. Brunschwig and N. Sutin, *The Journal of Physical Chemistry B*, 2005, **109**, 10251-10260.
55. G. R. Buettner and B. A. Jurkiewicz, *Free Radical Biology and Medicine*, 1993, **14**, 49-55.
56. C. Creutz, N. Sutin and B. S. Brunschwig, *Journal of the American Chemical Society*, 1979, **101**, 1297-1298.
57. R. A. Marcus, *Reviews of Modern Physics*, 1993, **65**, 599-610.
58. M. Braun, S. Atalick, D. M. Guldi, H. Lanig, M. Brettreich, S. Burghardt, M. Hatzimarinaki, E. Ravanelli, M. Prato and R. van Eldik, *Chemistry-A European Journal*, 2003, **9**, 3867-3875.

A self-assembled and spatially-separated donor-acceptor complex $Ru(bpy)_3^{2+}$-polymer-Pt shows high efficiency of hydrogen evolution at an apparent quantum yield of 12.8 % under visible light irradiation.